AMERICAN SOCIETY FOR MICROBIOLOGY | Infection and Immunity

Bacteriophages | Full-Length Text

Inflammation plays a critical role in damage to the bronchiolar epithelium induced by *Trueperella pyogenes in vitro* and *in vivo*

Lei Qin,[1,2] Fandan Meng,[1] Haijuan He,[3] Siqi Li,[1] Hongliang Zhang,[1] Yuan Sun,[1] Wenlong Zhang,[4] Tongqing An,[1] Xuehui Cai,[1,5] Shujie Wang[1,6]

AUTHOR AFFILIATIONS See affiliation list on p. 15.

ABSTRACT *Trueperella pyogenes* can cause severe pulmonary disease in swine, but the mechanism of pathogenesis is not well defined. *T. pyogenes*-induced damage to porcine bronchial epithelial cells (PBECs), porcine precision-cut lung slices (PCLS), and respiratory epithelium of mice remains unknown. In this study, we used *T. pyogenes* 20121 to infect PBECs in air-liquid interface conditions and porcine PCLS. *T. pyogenes* could adhere to, colonize, and induce cytotoxic effect on PBECs and the luminal surface of bronchi in PCLS, which damaged the bronchiolar epithelium. Moreover, bronchiolar epithelial cells showed extensive degeneration in the lungs of infected mice. Furthermore, western blot showed that the NOD-like receptor (NLR)/C-terminal caspase recruitment domain (ASC)/caspase-1 axis and nuclear factor-kappa B pathway were involved in inflammation in PCLS and lungs of mice, which also confirms that porcine PCLS provide a platform to analyze the pulmonary immune response. Meanwhile, the levels of p-c-Jun N-terminal kinase, p-extracellular signal-regulated kinase, and p-protein kinase B (AKT) were increased significantly, which indicated the mitogen-activated protein kinase and Akt pathways were also involved in inflammation in *T. pyogenes*-infected mice. In addition, we used *T. pyogenes* 20121 to infect tumor necrosis factor-alpha (tnf-$\alpha^{-/-}$) mice, and the results indicated that apoptosis and injury in respiratory epithelium of infected tnf-$\alpha^{-/-}$ mice were alleviated. Thus, the pro-inflammatory cytokine TNF-α played a role in apoptosis and the respiratory epithelium injury in mouse lungs. Collectively, our study provides insight into the inflammatory injury induced by *T. pyogenes* and suggests that blocking NLR may be a potential therapeutic strategy against *T. pyogenes* infection.

KEYWORDS *Trueperella pyogenes*, PBECs, PCLS, infection, inflammation, intracellular pathways

Trueperella pyogenes is frequently isolated from pyogenic disease conditions in both domestic and wild animals worldwide, but it is rare in companion animals and humans. *T. pyogenes* also plays an important role in secondary infection and co-infection in domestic animals (1, 2). In swine, *T. pyogenes* is a common opportunistic pathogen found in pneumonia, endocarditis, pleuritis, and organ abscesses (3, 4), and it is an emerging clinical, epidemiological, and economic problem on pig farms (5). Although pneumonia in swine with airway inflammation caused by *T. pyogenes* is frequent (6), the mechanisms of pathogenesis remain poorly understood.

The primary route of infection for many respiratory pathogens is the airway, which is lined by a layer of epithelial cells that form a primary barrier (7). Thus, well-differentiated porcine bronchial epithelial cells (PBECs) in air-liquid interface (ALI) conditions, which provide a close *in vitro* model of the airway epithelium (8, 9), have been used to study bacterial infections (10, 11). Precision-cut lung slices (PCLS) as *ex vivo* lung culture can mimic the immediate and long-term functional responses of the respiratory tract and lung (12–14), which allows studies on inflammatory responses induced by respiratory

Editor Kimberly A. Kline, Universite de Geneve, Geneva, Switzerland

Address correspondence to Xuehui Cai, caixuehui@caas.cn, or Shujie Wang, wangshujie@caas.cn.

Lei Qin and Fandan Meng contributed equally to this article. Author order was determined alphabetically.

The authors declare no conflict of interest.

See the funding table on p. 15.

Received 21 July 2023
Accepted 26 September 2023
Published 6 November 2023

pathogens (15, 16). Moreover, the 3D respiratory organotypic tissue reflects the natural microanatomy and microenvironment of the respiratory system (14), permitting a reduction in the number of laboratory animals used.

Little is known about the inflammatory response and mechanism of bronchial damage of *T. pyogenes* infections *in vitro* or *in vivo*, though we recently used PCLS to study the pathogenicity of a novel isolate (17). In the present study, ALI cultures, PCLS, and mice were used to analyze the adherence and colonization of *T. pyogenes* to porcine airway epithelial cells, seeking to further elucidate how the bacterium damages the respiratory tract.

MATERIALS AND METHODS

Bacterial strain and growth conditions

The virulent strain *T. pyogenes* 20121 was isolated from the lungs of sick pigs from a pig farm as previously described (17) and stored in our lab. *T. pyogenes* 20121 was grown at 37°C in tryptic soy broth (TSB; Difco, Loveton Circle Sparks, MD, USA) supplemented with 5% fetal bovine serum (FBS; Clark, USA) or on Columbia-based blood agar media (ThermoFisher Scientific, China). For the preparation of cryo-conserved bacterial stocks, *T. pyogenes* was grown in the TSB medium until the late exponential growth phase (OD_{600nm} = 0.5). Bacteria were harvested by centrifugation (3,000 × *g* for 5 min at 4°C), washed once with phosphate-buffered saline (PBS), and re-suspended in TSB medium containing 50% (vol/vol) glycerol. Aliquots were immediately flash frozen in liquid nitrogen and stored at −80°C until use.

Infection of well-differentiated PBECs by *T. pyogenes*

Porcine lungs were obtained from specific-pathogen-free (SPF) pigs, and primary PBECs were harvested from the bronchi as previously described (11). Briefly, PBECs were scraped carefully from the luminal surface of the bronchus without disturbing the mucosal surface integrity and cultured in bronchial epithelial cell growth medium (BEBM; Lonza, Belgium) supplemented with Abx (80 µg/mL kanamycin, 10 µg/mL enrofloxacin, 5 µg/mL levofloxacin, 2.5 µg/mL amphotericin, and 50 µg/mL ciprofloxacin). When PBECs reached about 80% confluence, they were seeded on 0.4 µm pore size transwell filters with polycarbonate membranes (Corning Costar, USA). Cells were then cultured at 37°C with 5% CO_2 in ALI medium, which is a mixture of BEBM and DMEM at 1:1 supplemented with Abx as described previously (18). At 3 days post-seeding, cultures were maintained under ALI conditions using media that were not supplemented with FBS for an additional 4 weeks at 37°C with 5% CO_2 for epithelial cell differentiation, changing the culture medium every 2 days.

Growth characteristics of *T. pyogenes* 20121 were determined on PBECs cultured under ALI conditions for 4 weeks, and all treatments were repeated at least three times. Transwell filters were washed three times with PBS and cultured in fresh medium without antibiotics for 24 h prior to infection. *T. pyogenes* 20121 was inoculated into the apical compartment with approximately 8×10^5 CFU per filter, and supernatant from the apical compartment was collected for a cytotoxicity assay after 4 h at 37°C with 5% CO_2. Both apical and basolateral compartments were washed three times with PBS to remove any non-adherent bacteria and maintained under ALI conditions. Cytotoxicity assays and immunofluorescence on PBECs were performed at 4, 24, 48, and 72 h post-inoculation (hpi).

Infection of *T. pyogenes* on porcine PCLS

The cranial, middle, and intermediate lobes were harvested from fresh lung tissue of three sacrificed SPF pigs. Each lobe was gently filled with warm 1.5% (wt/vol) low-melting agarose (Promega, USA) along the bronchus as described previously (19). The lobes were stamped out with an 8-mm tissue coring tool, and after the agar solidified, slices

were prepared on a Krumdieck tissue slicer (model MD6000-01; TSE Systems, USA) with 6–10 slices per min. Next, the PCLS were carefully transferred into 24-well plates and maintained with 1 mL fresh RPMI medium 1640 supplemented with Abx, and the medium was refreshed each hour to remove the agarose and repeated three times, then cultured overnight. PCLS containing bronchia and showing 100% ciliary activity were selected by light microscopy (EVOS FL Auto; Thermo Fisher Scientific, USA) for subsequent experiments. RPMI medium 1640 without antibiotic or antimycotic was added 24 h prior to bacterial infection studies. PCLS were washed three times with PBS, then inoculated with *T. pyogenes* at 8×10^4 ($n = 3$ slices) or 8×10^5 CFU ($n = 3$ slices) per slice at 37°C, and the control group (mock-infected, $n = 6$ slices) was cultured normally under the same conditions. The experiment was repeated three times ($n = 1$ pig per repeat, three pigs total). At 4 hpi, slices were washed three times with PBS to remove non-attached bacteria, and 1 mL fresh RPMI medium 1640 (Gibco, Beijing, China) was added for further cultivation. The supernatant was collected at 4, 24, and 72 hpi for cytotoxicity assays, and PCLS were homogenized in PBS and then serially diluted and plated onto tryptic soy agar (TSA) for the enumeration of bacteria.

Cytotoxicity assay

The release of lactate dehydrogenase (LDH, Promega, USA) into the culture medium was quantitated using Cyto Tox 96 Non-Radioactive Cytotoxicity Assay (Promega, Madison, WI, USA) as described previously (20). To determine the cytotoxic effect caused by *T. pyogenes* 20121, 50 µL of supernatant from infected or mock-infected PBECs or PCLS at each time point was mixed with an equal volume of substrate mix reagent in the dark. The detected supernatant in PBECs was obtained by washing the upper chamber of the transwell for 20 min using a culture medium on the shaker at 24, 48, and 72 hpi. After 30 min, stop solution was added and the absorbance signal was measured at 490 nm. The results were compared with the control group and presented as 100% cytotoxicity. Three parallel PBECs or PCLS (from the same pig) in different infected groups were collected at each detection time, and the infected experiments were repeated three times (one pig per repeat, three pigs total). The cytotoxicity assays in PBECs or PCLS were replicated three times.

Animal experiments

Seven-week-old female C57BL/6 wild-type (WT) mice (Changsheng Biotechnology, Liaoning, China) were randomly divided into two groups. Uninfected controls ($n = 12$) received 0.2 mL TSB intraperitoneally (i.p.), and the rest ($n = 20$) were challenged i.p. with 0.2 mL TSB containing 2×10^6 CFU *T. pyogenes* 20121. Lung and blood samples (collected with and without anticoagulant) from infected mice ($n = 5$) and controls ($n = 3$) were aseptically harvested after 1-, 2-, 4-, and 7-days post-infection (dpi) for histopathological and western blot analysis. Blood without anticoagulant was left at room temperature for 2 h and centrifuged at 5,000 × *g* for 10 min, then the serum was collected for cytokine detection. Bacterial load in lungs and anticoagulant-treated blood were monitored as previously described (21); briefly, anticoagulant-treated blood and lung samples were serially diluted and plated on blood agar medium for 36 h, and the bacteria were quantified by colony counting.

In a separate experiment, 16 female tnf-$\alpha^{-/-}$ C57BL/6N mice were purchased from Cyagen Biosciences (Santa Clara, USA) and were randomly divided into two groups at 6–7 weeks of age. Uninfected controls ($n = 6$) received 0.2 mL TSB i.p., and the other group was inoculated i.p. with *T. pyogenes* 20121 as above. Five infected tnf-$\alpha^{-/-}$ mice and three uninfected tnf-$\alpha^{-/-}$ mice were humanely euthanized at 1 and 2 dpi, lung and blood samples were harvested, and lung tissue samples were fixed in 3.7% formaldehyde (Amresco, Fountain Parkway, USA) for further histopathological analysis. Lung samples were sectioned (8-µm-thick slices) on a cryostat and used for double-immunofluorescence staining.

Cryosections and immunofluorescence analysis

Bronchoconstriction induced by *T. pyogenes* was detected by imaging based on the measurement of the bronchial cavity area. Initial bronchial cavity area was calculated for each PCLS by imaging at 0 hpi by inverted light microscope (EVOS FL Auto, ThermoFisher Scientific) and measured by ImageJ/Fiji software using a previous method (17), and bronchial contraction percentage (BCP) was calculated using the following formula: BCP = (final bronchial cavity area/initial bronchial cavity area) × 100%. For the cryosections, PCLS were washed three times using PBS to remove unattached bacteria, embedded on filter paper by tissue freezing medium (Sigma-Aldrich, USA), and quickly frozen in liquid nitrogen, then stored at −80°C. Ten micrometer-thick cryo-slices were produced by a cryostat (Thermo, USA) and stored at −20°C. The slices were dried at room temperature (RT) prior to immunofluorescence analysis.

PBECs and cryosection samples were fixed with 3.7% paraformaldehyde (Amresco, Fountain Parkway, USA) for 30 min, followed by 0.1 M glycine treatment for 20 min at RT. After three washing steps with PBS, samples were permeabilized with 0.2% Triton X-100 (Sigma-Aldrich, USA) for 20 min at RT. To block nonspecific reactions, 1% (vol/vol) bovine serum albumin (BSA; biofroxx, Germany) was used for 30 min at RT. The primary antibody for the detection of *T. pyogenes* was polyclonal mouse antiserum (1: 300, made in our lab), and ciliated cells were stained using a Cy3-labeled anti-β-tubulin monoclonal antibody (1:300; Sigma-Aldrich, USA). Alexa Fluor 488-labeled goat-anti-mouse IgG (H + L) (1:1,000, Thermo Fisher Scientific, USA) was used as a secondary antibody; all antibodies were diluted in 1% BSA. Nuclei were stained with DAPI (4′,6-diamidino-2-phenylindole; Cell Signaling Technology, USA), and finally, samples were mounted with ProLong Gold Antifade Reagent (Thermo Fisher Scientific, USA) and stored at 4°C with light protection. Slides were examined on a confocal laser scanning microscope with fast Airyscan (LSM980-ZEISS, Germany), and Z-stack images were acquired containing 0.22 µm per plane. Maximum intensity projections were calculated for display purposes and adjusted for brightness and contrast using ZEN 2.3 blue software.

Lung samples collected at necropsy were sectioned (7-µm-thick) and used for apoptosis detection. To confirm the cells of lungs that underwent apoptosis, lung sections of WT mice or tnf-$\alpha^{-/-}$ mice at 2 dpi were detected using a terminal deoxynucleotidyl transferase-mediated deoxyuridine triphosphate-biotin nick end-labeling (TUNEL) assay with Cell Death Detection Kit (Roche, Germany). Nuclei were stained with 4-6-diamidino-2-phenylindole (DAPI, Sigma).

Western blot analysis

Lung samples from the PCLS and mice were lysed in Radio Immunoprecipitation Assay (RIPA) lysis buffer (Beyotime, China), containing the protease inhibitors phenylmethanesulfonyl fluoride (PMSF) (Solarbio, China) and Complete Protease Inhibitor (EDTA-free; Merck-Millipore, Germany). Protein concentration was quantified using a BCA Protein Assay Kit (Beyotime Institute of Biotechnology, China). Equal amounts of protein were loaded and separated by electrophoresis on 12% SDS-PAGE gels and subsequently transferred to polyvinylidene fluoride (Merck-Millipore, Germany). After blocking with 10% skim milk for 1 h, the membranes were incubated at room temperature for 1 h with antibodies targeting the inflammasome, including rabbit antibodies against NLRP1, NLRC4, gasdermin D (GSDMD), GSDMD-C (1:1,000, abcam), interleukin (IL)-1β, IL-4, IL-18, matrix metalloproteinase 9 (MMP9), macrophage migration inhibitory factor (MIF) (1:500, ABclonal), NLRP3, caspase-1 p20, and mouse antibodies against ASC (1:1,000, these three antibodies were kindly provided by Professor Changjiang Weng of Harbin Veterinary Research Institute of Chinese Academy of Agricultural Sciences (22)). The rabbit anti-AKT1/2/3 and phosphor-AKT1/2/3, p38 and phospho-p38, ERK1/2 and phospho-ERK1/2, JNK1/2/3 and phospho-JNK1/2/3, NF-κB p65 and phospho-NF-κB p65 (1:1,000, abcam) were prepared for the tests of MAPK, Akt, and nuclear factor-kappa B (NF-κB) signaling pathways. Furthermore, antibodies targeting factors related to apoptosis including rabbit antibodies against caspase-8, caspase-9, caspase-3,

and apoptosis-inducing factor (AIF) (1:1,000, abcam) were also used in this process. Expression of all target proteins was normalized to that of the internal control rabbit/mouse antibodies against β-actin or GADPH (1:50,000, ABclonal). Relevant DyLight 800-labeled goat anti-rabbit/-mouse IgG (H + L) secondary antibodies were applied as needed (SeraCare, KPL Antibodies & Conjugates, USA). The relative integrated density of the target protein to the internal control was quantified using Image J v1.8.0 software (Wayne Rasband, National Institutes of Health, USA), and the relative quantitative comparison was shown after normalization of the relative integrated density of the control group.

Detection of cytokine production in PCLS or mice

To quantify the cytokines induced by *T. pyogenes* infection, supernatants from infected PCLS were collected at 4, 24, and 72 hpi, and the quantities of IL-4, IL-10, and chemokine CXCL8 were determined by ELISA according to the manufacturer's instructions (USCN Life Sciences, China). The quantities of IL-1β, IL-6, IL-10, TNF-α, and IFN-γ were also determined in serum samples collected from infected mice at 1, 2, 4, and 7 dpi by commercial ELISA according to the manufacturer's instructions (Cusabio, China).

Statistical analyses

All experiments were performed at least three times, and the results are expressed as the mean ± standard deviation (SD). Statistical analysis of the results was performed with one- or two-way analysis of variance (ANOVA) using GraphPad Prism software version 9.00 (GraphPad, San Diego, CA, USA). A P value < 0.05 was considered statistically significant.

RESULTS

T. pyogenes infection induces epithelium damage on well-differentiated PBECs

The infection of well-differentiated PBECs by *T. pyogenes* was first analyzed under ALI conditions. *T. pyogenes* induced cytotoxic effects as early as 4 hpi in comparison to mock-infected PBECs (Fig. 1A). No significant cytotoxic effect was detected at 24 hpi in comparison to mock-infected PBECs, but cytotoxic effect was significantly enhanced at 48 hpi. Attachment of *T. pyogenes* to epithelial cells under ALI conditions was detected by confocal microscopy (Fig. 1B). Tiny microcolonies of *T. pyogenes* were observed adhering to the cilia of the ciliated cell at 4 hpi. The size of these microcolonies increased by 24 hpi, indicating *T. pyogenes* was able to proliferate on the epithelial cells under ALI conditions. Notably, *T. pyogenes* caused severe damage to the epithelial cells and the cilia after infection, and epithelial integrity was lost by 72 hpi. Importantly, *T. pyogenes* crossed the epithelial cell layer and reached the membrane of the transwell filter.

Adhesion and colonization of *T. pyogenes* on the luminal surface of bronchi in porcine PCLS

To investigate the adhesion and colonization characteristics, porcine PCLS were infected or mock-infected by *T. pyogenes* 20121. Bronchoconstriction was induced by bacterial infection in a dose-dependent manner (Fig. 2A). At 8×10^5 CFU/slice, *T. pyogenes* caused notable bronchoconstriction (BCP: 94.46%, 87.18%, and 84.91%, respectively), while slighter constriction (BCP: 62.69%, 70.09%, and 75.02%, respectively) was seen with 8×10^4 CFU/slice at 4, 24, and 72 hpi. *T. pyogenes* adhered in microcolonies to the luminal surface of bronchi that was presented by the cilia of ciliated epithelial cells (shown in red) (Fig. 2A). Growth of *T. pyogenes* was not affected by bronchoconstriction, with colonizing bacteria still able to proliferate in the constricted area of bronchioles, as indicated by the arrow (Fig. 2A, 24 hpi). Infection with 8×10^5 CFU of *T. pyogenes* also caused more severe injury to the ciliated epithelial layer than the lower dose at 72 hpi (Fig. 2A). Meanwhile,

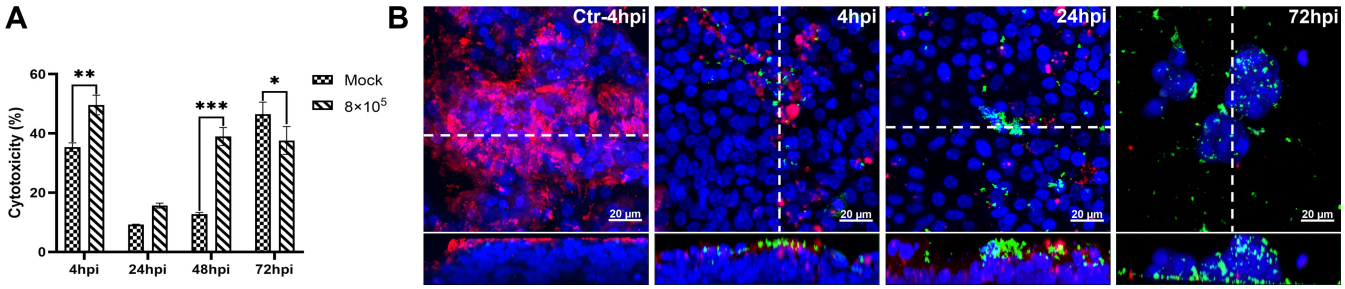

FIG 1 Cytotoxicity and *T. pyogenes*-induced damage to well-differentiated porcine bronchial epithelial cells. PBECs were apically infected with approximately 8 × 10^5 CFU of *T. pyogenes* and washed thoroughly after 4 h to remove non-adherent bacteria, then further incubated under ALI conditions. (A) Cytotoxic effects of *T. pyogenes* on PBECs grown under ALI conditions were quantified by a standard LDH-release assay. Results are expressed as percent cytotoxicity compared to 100% killed cells condition and expressed as mean ± SD; **P* < .05, ***P* < .01, ****P* < 0.001, determined using one-way ANOVA and Tukey's multiple comparison test. Experiments were performed three times. (B) Immunostaining was performed to visualize cilia (red) and *T. pyogenes* (green), and nuclei were stained by DAPI (blue). Bars represent 20 µm in horizontal sections for upper images, and lower images are the orthogonal views of Z-stacks (white dotted line) as shown in YZ sections at 4 and 72 hpi or XZ sections in control (Ctr) at 4 and 24 hpi.

the CFU counts in PCLS slice lysates also showed much higher numbers at 24 and 72 hpi than at 4 hpi (Fig. 2B), confirming the proliferation of *T. pyogenes*. Additionally, the 8 × 10^5 CFU-infected group had more bacteria attached (>10^5 CFU) compared with the 8 × 10^4 CFU-infected group (10^4 CFU) at 24 hpi, whereas no significant difference was detected at 72 hpi.

As a measure of cytotoxicity, the amount of LDH released from infected PCLS was determined. *T. pyogenes* induced significant cytotoxic effect on PCLS at 4 and 24 hpi, and the high-dose group showed greater cytotoxicity than the low-dose group (Fig. 2C). The low-dose infection group caused slightly higher cytotoxicity than the high-dose group at 72 hpi, which may be related to a decrease in the number of surviving ciliated epithelial cells due to the more serious damage caused by the high-dose infection.

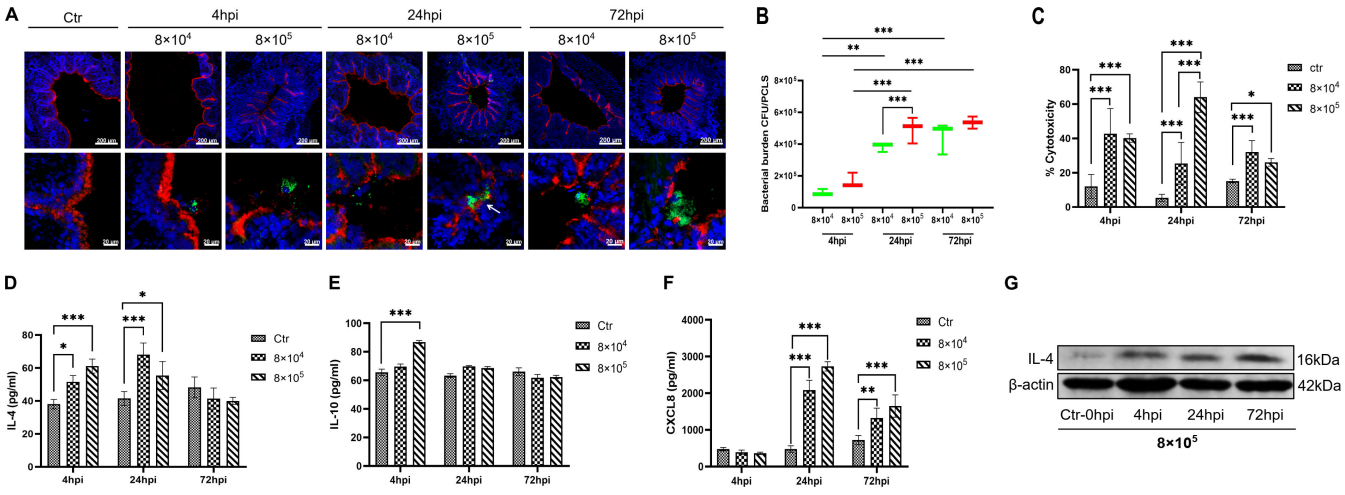

FIG 2 Interaction between *T. pyogenes* with porcine precision-cut lung slices. PCLS were infected with 8 × 10^4 or 8 × 10^5 CFU/well of *T. pyogenes* for 4 h and washed thoroughly to remove non-adherent bacteria. Cells were fixed for cryosections at 4, 24, and 72 hpi and used for immunofluorescence staining. (A) *T. pyogenes* is shown in green, cilia (β-tubulin) in red, and nuclei (DAPI) in blue. (B) Bacterial burden of *T. pyogenes* on PCLS at 4, 24, and 72 hpi. (C) *T. pyogenes*-induced cytotoxicity on PCLS, expressed as percent cytotoxicity compared to 100% killed cells condition. (D) IL-4 and (E) IL-10 levels in PCLS supernatant after incubation with *T. pyogenes*. (F) ELISA was used to determine the level of chemokine CXCL8 in the culture supernatant. (G) Western blot analysis was used to determine the amount of IL-4 in the infected PCLS at 4, 24, and 72 hpi. The PCLS from three pigs and experiments were performed three times; **P* < 0.05, ***P* < 0.01, and ****P* < 0.001.

Secretion of inflammatory cytokines into the supernatant of infected porcine PCLS

To understand the immune response triggered by *T. pyogenes* in PCLS, the amount of cytokines released into the supernatant was measured. Secretion of anti-inflammatory cytokines IL-4 and IL-10 in the supernatant (Fig. 2D and E) was observed at 4 hpi, which proceeded to the secretion of the chemokine CXCL8 (Fig. 2F). The level of IL-4 in supernatant of both infected groups was significantly higher ($P < 0.001$) than mock infection at 4 and 24 hpi, and IL-10 increased significantly by 4 hpi only in the high-dose group. Western blot analysis also confirmed upregulation of IL-4 in PCLS tissue infected with 8×10^5 CFU at 4, 24, and 72 hpi (Fig. 2G). However, CXCL8 was notably upregulated in the supernatant of *T. pyogenes*-infected PCLS by 24 and 72 hpi compared with mock infection.

T. pyogenes activated the NLRP3 and NF-κB pathways in porcine PCLS

To investigate the effect of the NLRP3 inflammasome on the *T. pyogenes*-induced inflammatory response, PCLS were collected for western blot analysis. *T. pyogenes* infection increased the expression of NLRP3 protein from 4 to 72 hpi (Fig. 3A), and ASC expression was also enhanced compared with the control (Fig. 3B). Meanwhile, pro-caspase-1 was activated and cleaved, with caspase-1 (p20) enhanced significantly at 24 and 72 hpi (Fig. 3C). Furthermore, the expression of inflammatory cytokines IL-1β and IL-18 was upregulated from 4 to 72 hpi relative to controls, but with a slight drop at 72 hpi compared with 24 hpi (Fig. 3D and E). In addition, NF-κB and two important factors that participate in inflammation (MMP9 and MIF) were analyzed. Expression of MMP9 increased significantly from 4 to 72 hpi (Fig. 3F) and expression of MIF increased strikingly at 24 and 72 hpi (Fig. 3G) compared with controls. Expression of NF-κB increased substantially at 24 and 72 hpi compared with controls. These results suggest that the NLRP3 inflammasome and NF-κB pathways are both activated in PCLS infected with *T. pyogenes*.

T. pyogenes damages the respiratory tract of infected mice

To examine the effect of *T. pyogenes* infection on the development of associated pulmonary pathology in a live animal model, 6-week-old C57BL/6 mice were i.p. inoculated with *T. pyogenes* or TSB, and the histopathological changes in the lungs or tracheae were examined at 1, 2, 4, and 7 dpi. The lungs of *T. pyogenes*-infected mice exhibited mild degeneration of bronchiolar epithelial cells with marked infiltration of inflammatory cells in the bronchial epithelium at 1 and 2 dpi (Fig. 4A). Furthermore, the bronchiolar epithelial cells were extensively degenerated at 4 dpi, and the adventitia showed mild edema in addition to degeneration of bronchiolar epithelial cells at 7 dpi. Compared with mock-infected mice, massive degeneration of tracheal epithelial cells was observed in mice infected with *T. pyogenes* from 1 to 4 dpi, and nuclear concentration of tracheal epithelial cells was observed at 7 dpi (Fig. 4B). Thus, *T. pyogenes* infection caused a significant inflammatory response and damage in the respiratory tract of mice.

Bacterial load and inflammatory cytokines in the blood of mice infected by *T. pyogenes*

The dynamic of bacterial load in the peripheral blood of infected mice was also investigated. In agreement with our previous report (17), no bacteria were detected in the blood during the first 2 days of infection, while bacteria were detectable at 4 dpi (66.67 CFU/mL) and increased substantially by 7 dpi (366.67 CFU/mL) (Fig. 5A). However, bacterial loads in the lungs could be detected at 1 and 2 dpi (1.44×10^5 CFU/g and 1.58×10^5 CFU/g, respectively), and bacterial levels increased strikingly at 4 and 7 dpi (4.78×10^5 and 2.39×10^6 CFU/g, respectively).

It is well known that airway contraction and inflammatory responses are regulated by multiple cytokines (22). To investigate the effect of *T. pyogenes* on cytokine production in

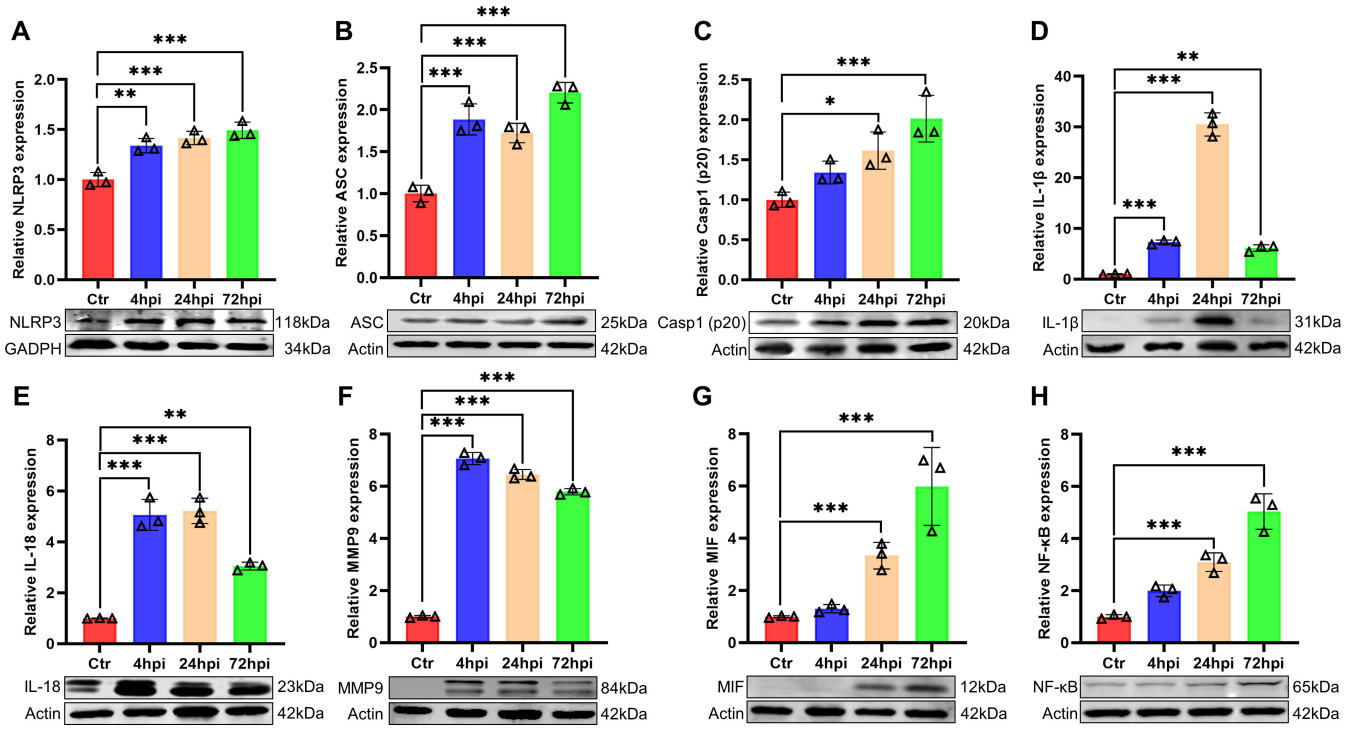

FIG 3 The NLRP3 and NF-κB pathways were activated by *T. pyogenes* in porcine precision-cut lung slices. PCLS were challenged with 8×10^5 CFU/well of *T. pyogenes* 20121. Western blot analysis was used to detect the levels of NLRP3 (A), ASC (B), caspase-1 (p20) (C), IL-1β (D), IL-18 (E), MMP9 (F), MIF (G), and NF-κB (H). Relative protein expression levels were detected by Image J software and expressed as mean ± SD; *$P < 0.05$, **$P < 0.01$, and ***$P < 0.001$.

mice, typical pro- and anti-inflammatory cytokines in the serum were examined by ELISA kits. After *T. pyogenes* infection, IL-1β increased significantly at 1 dpi, then decreased at 2, 4, and 7 dpi compared to 1 dpi (Fig. 5B). IL-6 increased significantly at 1 dpi (24.89 pg/mL) and peaked at 2 dpi (34.50 pg/mL) (Fig. 5C). TNF-α and IFN-γ were both significantly increased at all time-points (Fig. 5D and E), with peaks at 4 dpi (247.34 pg/mL) and 1 dpi (865.29 pg/mL), respectively. IL-10 increased significantly ($P < 0.001$) at 4 and 7 dpi (Fig. 5F).

T. pyogenes activates inflammasome, MAPK, Akt, and NF-κB signaling pathways in the lungs of infected mice

To identify whether the inflammasome is activated in response to *T. pyogenes* infection, we used four different antibodies to detect inflammasome complexes in lung tissue by western blot (Fig. 6). The results showed that NLRP1 and NLRC4 protein expression (Fig. 6A and B) increased significantly between 2 and 7 dpi, while NLRP3 increased significantly only at 7 dpi (Fig. 6C) and AIM-2 was not expressed (data not shown), which suggests the NLRP1 and NLRC4 inflammasomes play a major role in early infection of mice. *T. pyogenes* clearly induced ASC expression and cleavage of pro-caspase-1, with both significantly increased from 1 to 7 dpi ($P < 0.001$) (Fig. 6D and E). Moreover, GSDMD expression decreased significantly between 2 and 7 dpi (Fig. 6F), whereas GSDMD-N and GSDMD-C were significantly increased from 1 to 7 dpi (Fig. 6G and H), suggesting that GSDMD was cleaved into GSDMD-N and GSDMD-C, then pyroptosis occurred and released numerous pro-inflammatory cytokines into the infected lungs. Indeed, western blot showed a marked increase in IL-1β and IL-18 (Fig. 6I and J) during infection, and MMP9 increased significantly at 1 dpi (Fig. 6K), whereas there was no significant change in MIF (Fig. 6L). Altogether, NLR inflammasomes were activated in the lung tissue of *T. pyogenes*-infected mice.

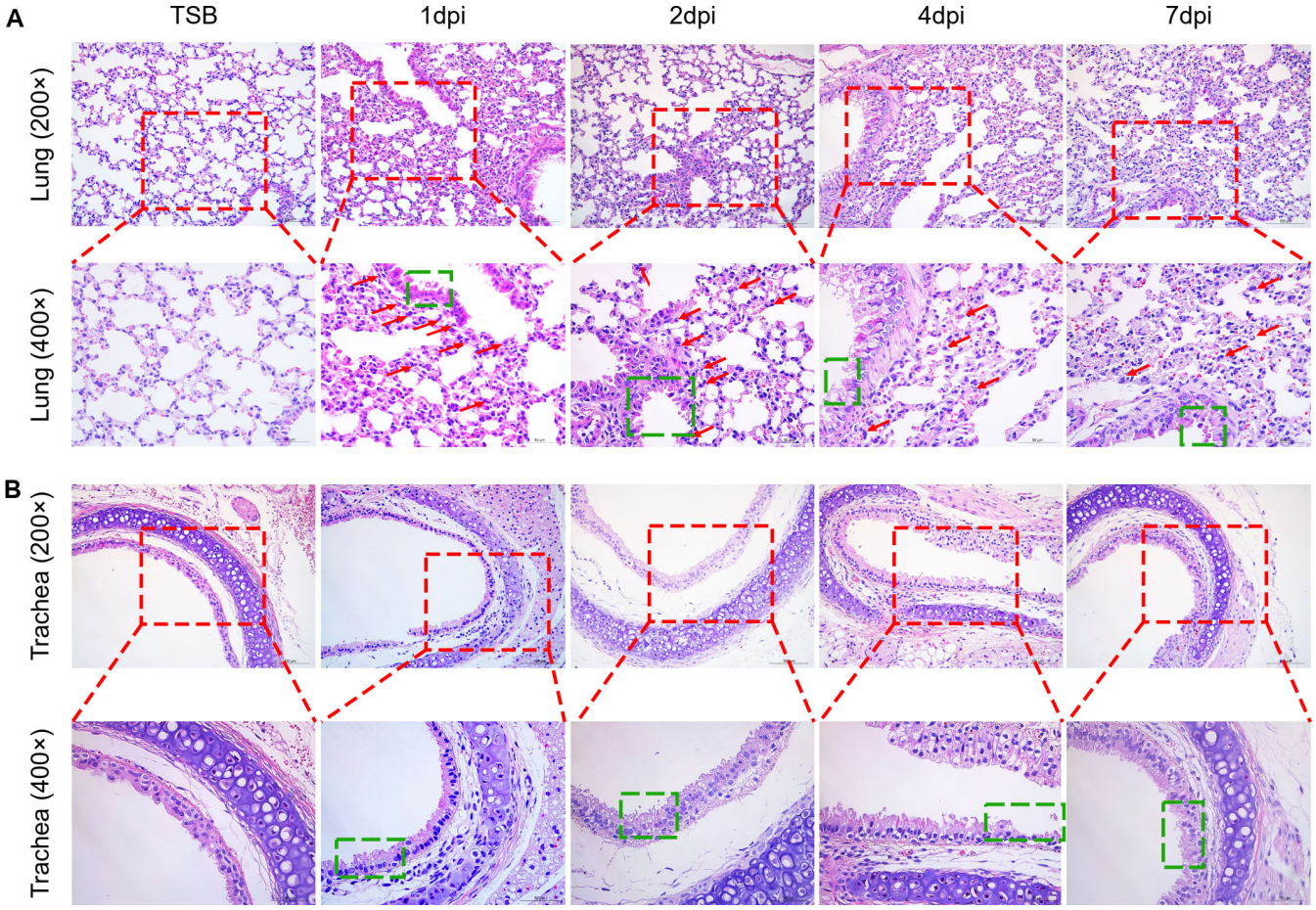

FIG 4 Histopathology lesions induced in the lungs of mice infected with *T. pyogenes*. Mice were infected with 2×10^6 CFU of *T. pyogenes* strain 20121 and sacrificed at 1, 2, 4, and 7 dpi. Samples of (A) lung and (B) trachea were fixed, embedded in paraffin, and sectioned at a thickness of 5 µm. Sections were stained with hematoxylin-eosin and photographed using Zeiss Viewer software; the red box shows greater detail, with extensive inflammatory cell infiltration of the lung (red arrow) and epithelial cell degeneration (green box).

In order to explore the mechanism of how *T. pyogenes* may induce inflammation, we also studied the effect of infection on the MAPK signaling pathways. Western blot was used to detect classical inflammation-related signaling kinases including JNK, ERK, and p38 of the MAPK pathway in the lungs of infected mice. The levels of p-JNK and p-ERK were increased and the ratio of p-JNK/JNK was increased significantly from 2 to 7 dpi (Fig. 7A), while the ratio of p-ERK/ERK and p-p38/p38 also increased significantly from 1 to 7 dpi (Fig. 7B and C). Moreover, we tested the activation status of the canonical Akt and NF-κB pathways, which are reported to be involved in the movement of immunocytes from the peripheral blood to sites of inflammation. The ratio of p-AKT/AKT was significantly increased throughout the study ($P < 0.01$) (Fig. 7D), and phosphorylation of NF-κB (Fig. 7E) was increased at 1, 4, and 7 dpi.

T. pyogenes infection induces apoptosis in the lungs of mice by both AIF-mediated and caspase-dependent pathways

A TUNEL assay was used to determine whether *T. pyogenes* induced apoptosis in the lungs of infected mice at 2 dpi. Apoptotic signals were found not only in bronchial epithelial cells but also in the alveoli (Fig. 8A and B), suggesting *T. pyogenes* could induce apoptosis in the lungs of infected mice. Next, we used western blot to determine which type of signaling was induced by *T. pyogenes* infection. As shown in Fig. 8C, the expression of AIF protein increased significantly at 1 and 2 dpi compared with the

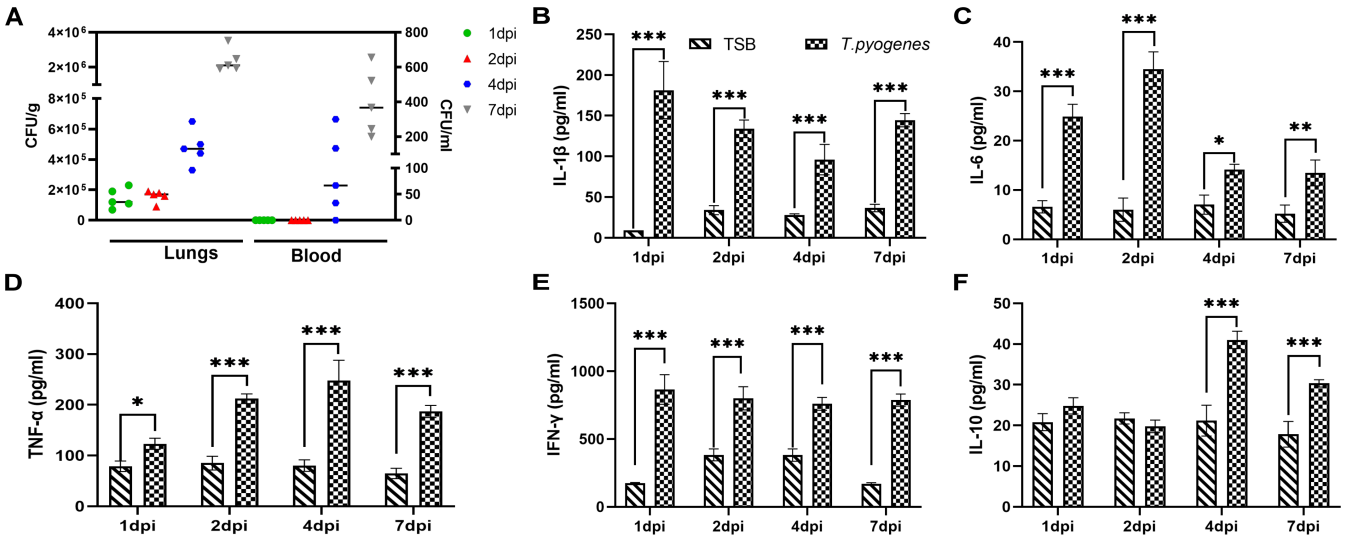

FIG 5 Bacterial load and cytokine levels in the lungs and blood of *T. pyogenes* -infected mice. (A) Bacterial load in the lung (CFU/g of tissue) and blood (CFU/mL). ELISA was used to detect the levels of (B) IL-1β, (C) IL-6, (D) TNF-α, (E) IFN-γ, and (F) IL-10 in serum samples. Data are shown as the mean ± SD of the independent experiments; **P* < 0.05, ***P* < 0.01, and ****P* < 0.001.

control group. In addition, there was a significant increase in caspase-3 and caspase-8 throughout the study (Fig. 8D and E). Meanwhile, cleaved caspase-3 also increased

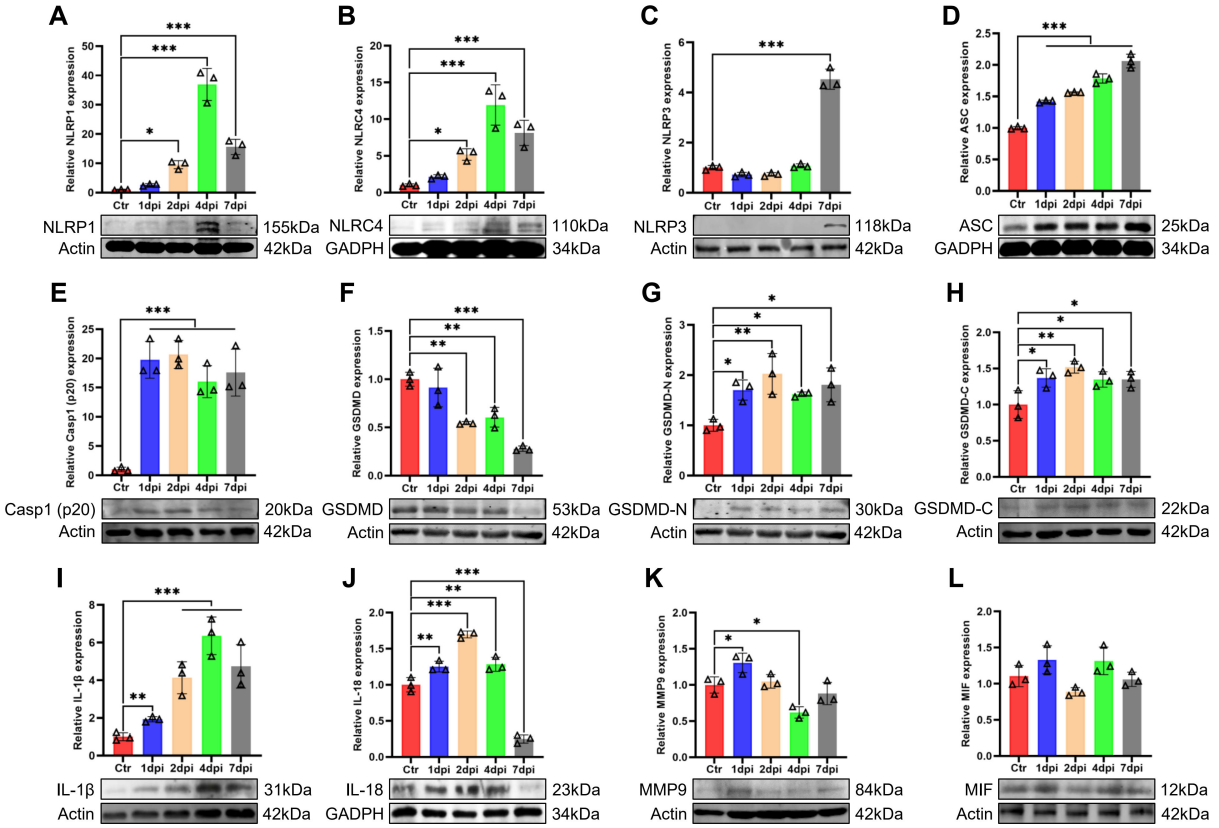

FIG 6 The NLR/ASC/caspase-1/IL axis is activated in the lungs of *T. pyogenes*-infected mice. Western blots of *T. pyogenes*-infected wild-type mouse lungs at 1, 2, 4, and 7 dpi are shown. Relative protein expression of (A) NLRP1, (B) NLRC4, (C) NLRP3, (D) ASC, (E) Casp1(p20), (F) GSDMD, (G) GSDMD-N, (H) GSDMD-C, (I) IL-1β, (J) IL-18, (K) MMP9, and (L) MIF are shown; **P* < 0.05, ***P* < 0.01, and ****P* < 0.001. The actin images (F and G) were reused here because they are parts of the same internally controlled experiment from the same gel.

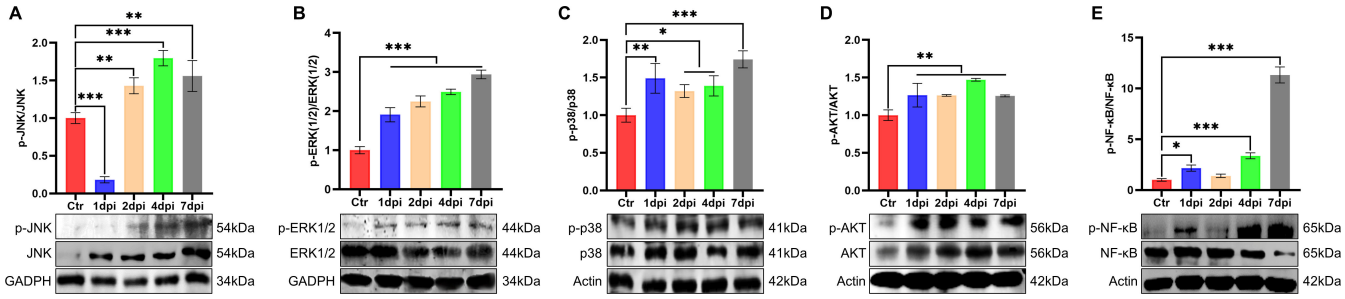

FIG 7 Comparison of protein expression of molecules related to activation of the MAPK pathway and inflammatory response in the lungs of mice after challenge with *T. pyogenes*. Representative western blots show the expression and phosphorylation level of (A) JNK, (B) ERK, (C) p38, (D) AKT, and (E) NF-κB. Densitometry analysis from three independent experiments was used to quantitate the protein expression, and the ratio of phosphorylated protein to total protein presented the relative expression results, and the values were normalized to the control value (relative density ratio). The mean ± SD of three experiments are shown; **P* < 0.05, ***P* < 0.01, and ****P* < 0.001.

significantly except 2 dpi and cleaved caspase-8 increased from 1 to 4 dpi (Fig. 8F and G), whereas caspase-9 had no significant change (Fig. 8H). These results suggest the involvement of an AIF-mediated apoptosis pathway and a caspase-dependent pathway in *T. pyogenes*-induced apoptosis.

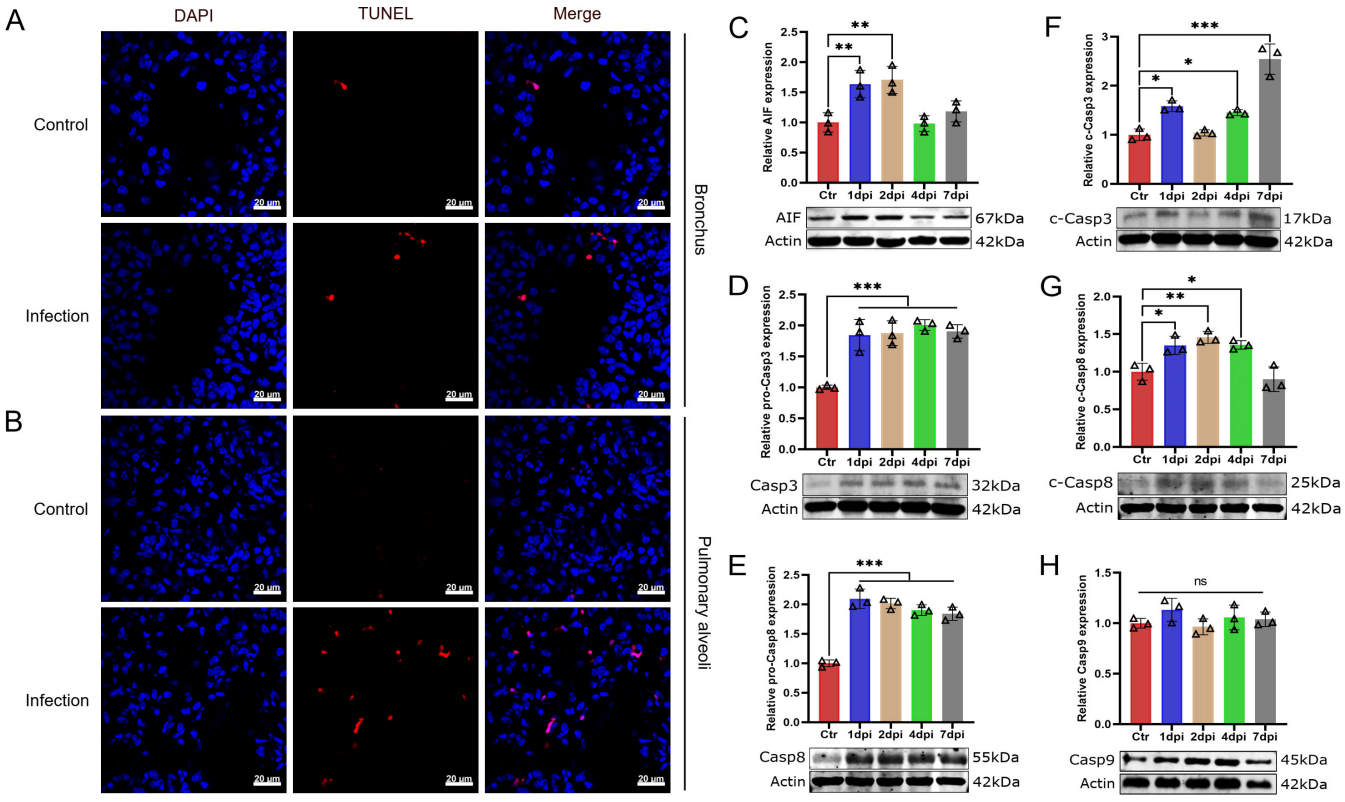

FIG 8 *T. pyogenes* infection induces apoptosis in mouse lung cells. (A) Mice were challenged with 2×10^6 CFU of *T. pyogenes*, and at 2 dpi, lungs were collected for immunofluorescence to verify the occurrence of apoptosis using a TUNEL assay. Apoptosis is shown in red in (A) bronchial epithelial cells and (B) pulmonary alveoli in the lung, and nuclei (DAPI) in blue. Western blot analysis of (C) AIF, (D) caspase-3 (Casp3), (E) caspase-8 (Casp8), (F) cleaved caspase-3 (c-Casp3), (G) cleaved caspase-8 (c-Casp8), and (H) caspase-9 (Casp9) expression shows apoptosis of lung cells at different days of infection. Data are shown as the mean ± SD of three experiments. **P* < 0.05, ***P* < 0.01, and ****P* < 0.001. The actin images including panels D and F and panels E and G were reused here because they are parts of the same internally controlled experiments from the same gel, respectively.

TNF-α plays a role in apoptosis and inflammatory injury in the bronchiolar epithelium

The level of caspase-8 increased significantly throughout at least the first 7 days of *T. pyogenes* infection, suggesting that the TNF signaling pathway may be activated. Thus, we infected tnf-α$^{-/-}$ mice to verify the role of TNF-α in apoptosis and lung damage. Apoptosis was detected using a TUNEL assay, and cell nuclei were stained with DAPI. As shown in Fig. 9A, there was lower apoptotic signal found in bronchial epithelial cells of tnf-α$^{-/-}$ mice at 2 dpi, and the number of apoptotic cells in the infected tnf-α$^{-/-}$ mice was significantly lower compared with the WT group (Fig. 9B). Furthermore, western blot analysis confirmed that the expression of caspase-8, caspase-3, and AIF decreased significantly compared with the WT group, whereas caspase-9 did not change significantly (Fig. 9C). Moreover, histopathologic analysis of lung and trachea of infected WT mice showed a large number of inflammatory cells infiltrated in the parenchyma of the lung on 2 dpi (Fig. 9D). Also, trachea mucosal epithelial cells were partially denatured, inflammatory cells infiltrated the submucosa, and the arrangement of bronchiolar/tracheal epithelial cells was more disordered compared with infected tnf-α$^{-/-}$ mice on 2 dpi.

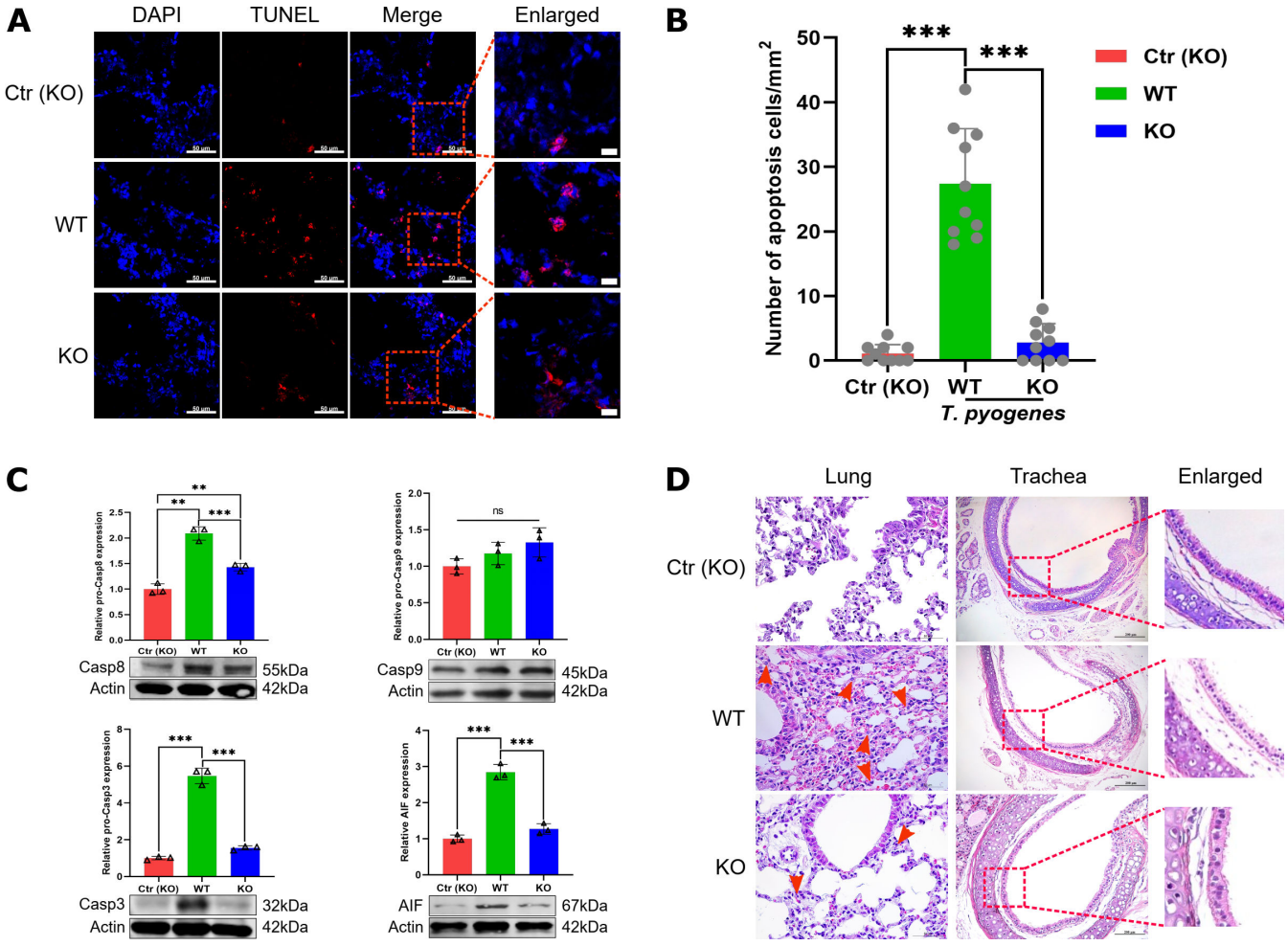

FIG 9 Comparison of apoptosis and injury induced by *T. pyogenes* alleviated in the lungs of wild-type and tnf-α$^{-/-}$ mice. WT and tnf-α$^{-/-}$ C57 (KO) mice were challenged with 2×10^6 CFU of *T. pyogenes*, and at 2 dpi, lungs were collected for immunofluorescence. (A) Apoptotic cells (TUNEL) in trachea epithelial cells were detected with the *In Situ* Cell Death Detection Kit, and cell nuclei were stained with DAPI. (B) Number of apoptotic cells in trachea epithelial cells from different groups of mice. ***$P < 0.001$. Protein levels of (C) caspase-8, caspase-9, caspase-3, and AIF were detected by western blot. (D) Comparison of histopathological lesions of lungs and trachea between infected WT and KO mice on 2 dpi, showing the epithelial layer of the respiratory tract of lungs (red dotted boxes) and neutrophils (red arrow).

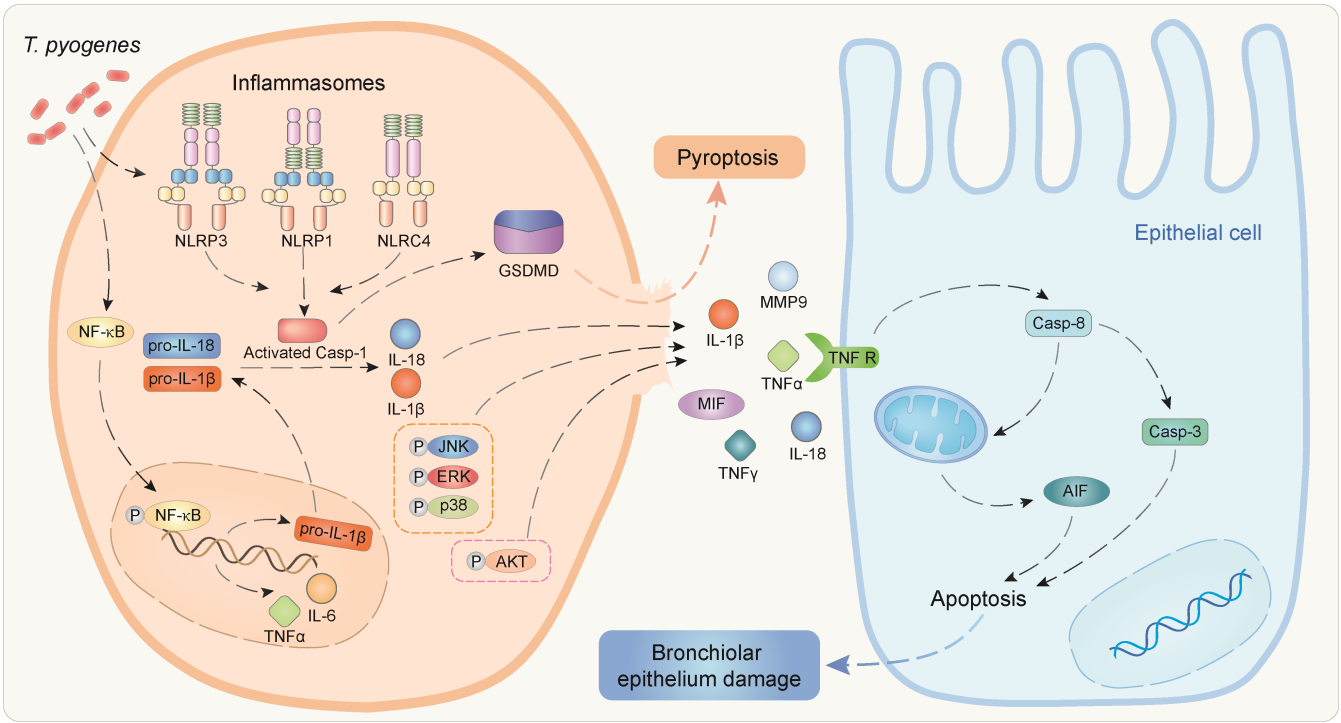

FIG 10 A schematic overview summarizing the main mechanism of epithelial cell injury. *T. pyogenes* infection triggers NF-κB to enter the nucleus, where it promotes the expression of pro-inflammatory factors and NLR inflammasomes. Meanwhile, *T. pyogenes* can directly promote the assembly and formation of the NLR inflammasome. Pyroptosis happens via the NLR-ASC-caspase-1-GSDMD pathway, which promotes the release of mature IL-18, IL-1β, and other pro-inflammatory factors into the extracellular space, which can cause inflammatory lung tissue injury. For example, TNF-α increases and induces epithelial cell apoptosis via the TNF receptor pathway.

In the infected tnf-α$^{-/-}$ mice, there was less inflammatory cell infiltration in the parenchyma of the lung compared with WT mice. Trachea mucosal epithelial cells showed slight degeneration and the arrangement of epithelial cells was more ordered than that seen with infection of WT mice on 2 dpi. Altogether, these data suggest that TNF-α plays a role in apoptosis and inflammatory injury to the bronchiolar epithelium of *T. pyogenes*-infected mice.

DISCUSSION

Currently, there have been few studies on the effect of *T. pyogenes* on lung functions *in vitro*. Well-differentiated PBECs and PCLS make it possible to analyze the host-pathogen interaction *in vitro*, including the initial events of immune activation (23). Here, we show that *T. pyogenes* is able to interact with PBECs and PCLS, inducing immune responses and developing airway damage.

In this study, notable bronchoconstriction was observed along with increased IL-4 in the supernatants of infected PCLS. Since IL-4 is associated with allergic disorders in humans (24), we speculate that its increase may contribute to bronchoconstriction. The mechanisms underlying IL-4 mediation of porcine bronchial constriction need to be further investigated. *T. pyogenes* could adhere to ciliated respiratory epithelial cells, growing either on the bronchial surface or within bronchoconstricted areas. Since bronchoconstriction can reduce the elimination capability of ciliated cells (25), *T. pyogenes*-induced bronchoconstriction may increase bacterial proliferation within constricted areas. Furthermore, *T. pyogenes* destroyed the integrity of the airway epithelium under ALI conditions, a property that may facilitate bacterial movement across the physical barriers of the respiratory epithelium. It has been reported that suilysin of *Streptococcus suis* can induce apoptosis of epithelial cells under ALI conditions

(10). As the genotype of *T. pyogenes* 20121 is *plo*$^+$/*fimA*$^+$/*fimE*$^+$/*nanH*$^+$/*nanP*$^+$ (17), hemolysin (pyolysin, plo) may accumulate locally in colonized areas under ALI conditions, inducing damage to epithelial cells. This will be further verified in future studies.

The release of LDH is used to measure cytotoxicity and pyroptosis. In this study, *T. pyogenes* induced cytotoxicity in well-differentiated PBECs (Fig. 1A) and PCLS (Fig. 2C) in a bacterial load-dependent manner. Non-adherent bacteria were removed at 4 hpi, and those attached were too few to induce a detectable cytotoxic effect at 24 hpi. As *T. pyogenes* proliferated, it reached a threshold to manifest cytotoxicity at 48 hpi. Increases in IL-1β, IL-18, and LDH in infected PCLS from 4 to 72 hpi are further evidence of pyrolysis and pyroptosis.

T. pyogenes usually produces a purulent-necrotic inflammation in the lung of clinically diseased swine (5), a process regulated by cytokines. Our results confirmed that *T. pyogenes* can induce pro-inflammatory cytokines and anti-inflammatory cytokines in PCLS and mice, which are related to the polarization of Th1 and Th2 cells. In infected mice, pro-inflammatory cytokines such as IL-1β, IL-6, TNF-a, and IFN-γ were produced in the serum, which suggests that Th1 cells are involved in the reaction to antigen. IL-10, a typical anti-inflammatory cytokine, was found in the serum of *T. pyogenes*-infected mice at significantly higher levels at 4 and 7 dpi but not at 1 and 2 dpi, which may be consistent with the inhibition of Th2-polarized responses by high Th1-related proinflammatory IFN-γ. Our results suggested *T. pyogenes* induces a strong pro-inflammatory response at the early stage of mice infection, but an anti-inflammatory process appears relatively late. However, the timing of IL-10 expression was different *in vitro* and *in vivo*, only significantly increasing in the 8×10^5 CFU-infected PCLS group at 4 hpi and not at 24 or 72 hpi. The specific mechanism remains to be further studied.

In this study, *T. pyogenes* infection of porcine PCLS and mice activated the inflammasome, which activated caspase-1 and promoted cleavage of pro-inflammatory mediators IL-1β and IL-18 into their mature states (Fig. 3). IL-1β and IL-18 are the most potent and first to be produced, binding to their receptors to recruit and activate other inflammatory cells. IL-1β and IL-18 increased significantly after *T. pyogenes* infection of PCLS and mice, along with MMP9 and MIF. At the site of inflammation, MMP9 is often found synchronous with IL-1β (26), and MIF is considered to have a strong pro-inflammatory effect (27). This is the first report that shows *T. pyogenes* can induce the secretion of pro-inflammatory cytokines in porcine PCLS. Meanwhile, the NF-κB pathway, which promotes the expression of pro-inflammatory cytokines including IL-6 and TNF-α, was activated in infected PCLS and mice (Fig. 10). The NLR-ASC-caspase-1 axis and NF-κB pathway were involved in both PCLS and mice, which confirm porcine PCLS provide a platform to analyze the early pulmonary immune response. In addition, the increased phosphorylation of JNK, ERK, and AKT in mice suggested the MAPK and Akt pathways were also involved in the observed inflammation (Fig. 10).

To better understand how TNF signaling is involved in the degeneration of epithelial cells of lungs in *T. pyogenes*-infected mice, we used tnf-α$^{-/-}$ mice, finding a lack of apoptosis and degeneration of epithelial cells in the lungs. Thus, pro-inflammatory TNF-α plays an important role in the apoptosis and lung injury induced by *T. pyogenes*. Collectively, *T. pyogenes* infection caused significant inflammatory responses in the respiratory system, releasing a variety of pro-inflammatory cytokines that were unrestricted by regulatory mediators, resulting in the degeneration of epithelial cells (Fig. 10). Blocking NLR inflammasome activation may prevent higher production of pro-inflammatory cytokines early in infection, which may slow the disease progression.

Conclusion

The role of inflammation in *T. pyogenes*-induced bronchiolar epithelium damage was investigated *in vitro* and *in vivo*, highlighting the mechanism underlying pathological development in the respiratory system during *T. pyogenes* infection. The NLR/ASC/

caspase-1/IL axis and NF-κB pathway play the greatest role in inflammation and contribute to bronchiolar epithelium damage during *T. pyogenes* infection.

ACKNOWLEDGMENTS

This work was supported by the National Natural Science Foundation of China (32273018), Heilongjiang Provincial Natural Science Foundation of China (LH2023C048), the Central Public-interest Scientific Institution Basal Research Fund (No. 1610302022006), and Foundation of Heilongjiang Educational Committee (2018-KYYWF-0109).

S.W., F.M., and X.C. conceived the study and designed the experimental procedures. L.Q., F.M., and S.L. performed the experiments. L.Q., F.M., H.H., W.Z., and S.W. analyzed the data. H.H., H.Z., Y.S., W.Z., T.A., and X.C. contributed reagents and materials. L.Q., F.M., and S.W. wrote the manuscript.

AUTHOR AFFILIATIONS

[1]State Key Laboratory for Animal Disease Control and Prevention, Harbin Veterinary Research Institute, Chinese Academy of Agricultural Sciences, Harbin, Heilongjiang, China
[2]Laboratory Animal Centre, Qiqihar Medical University, Qiqihar, China
[3]Institute of Animal Husbandry, Heilongjiang Academy of Agriculture Sciences, Harbin, Heilongjiang, China
[4]College of Veterinary Medicine, Northeast Agricultural University, Harbin, Heilongjiang, China
[5]Heilongjiang Research Center for Veterinary Biopharmaceutical Technology, Harbin, China
[6]Heilongjiang Provincial Key Laboratory of Veterinary Immunology, Harbin, China

AUTHOR ORCIDs

Tongqing An http://orcid.org/0000-0003-4619-4587
Xuehui Cai http://orcid.org/0000-0001-9098-7782
Shujie Wang http://orcid.org/0000-0002-7020-5410

FUNDING

Funder	Grant(s)	Author(s)
MOST | National Natural Science Foundation of China (NSFC)	32273018	Shujie Wang
Central Public-interest Scientific Institution Basal Research Fund	NO.1610302022006	Shujie Wang
Heilongjiang Provincial Natural Science Foundation of China	LH2023C048	Shujie Wang
Foundation of Heilongjiang Educational Committee	2018-KYYWF-0109	Lei Qin

AUTHOR CONTRIBUTIONS

Lei Qin, Data curation, Formal analysis, Methodology | Fandan Meng, Conceptualization, Funding acquisition, Methodology, Writing – original draft, Writing – review and editing | Haijuan He, Data curation, Formal analysis | Siqi Li, Methodology, Software | Hongliang Zhang, Methodology, Resources | Yuan Sun, Data curation, Methodology | Wenlong Zhang, Data curation, Methodology | Tongqing An, Data curation, Funding acquisition | Xuehui Cai, Funding acquisition, Methodology, Supervision | Shujie Wang, Conceptualization, Funding acquisition, Supervision, Writing – original draft, Writing – review and editing

ETHICS APPROVAL

All animal experiments were performed in accordance with the Guide for the Care and Use of Laboratory Animals of the Ministry of Science and Technology of the People's Republic of China. Mouse infection experiments (approval number 210119-02) were carried out in animal biosafety level 2 facilities under the supervision of the Committee on the Ethics of Animal Experiments of the Harbin Veterinary Research Institute of the Chinese Academy of Agricultural Sciences (CAAS) and the Animal Ethics Committee of Heilongjiang Province, China.

REFERENCES

1. Qi M, Liu J, Jiang Q, Niu H, Wang X, Zhou D, Lin P, Chen H, Wang A, Jin Y. 2021. *Trueperella pyogenes* pyolysin inhibits lipopolysaccharide-induced inflammatory response in endometrium stromal cells via autophagy- and ATF6-dependent mechanism. Braz J Microbiol 52:939–952. https://doi.org/10.1007/s42770-021-00422-5
2. Ahmed MFE, Alssahen M, Lämmler C, Eisenberg T, Plötz M, Abdulmawjood A. 2020. Studies on *Trueperella pyogenes* isolated from an okapi (*Okapia johnstoni*) and a royal python (*Python regius*). BMC Vet Res 16:292. https://doi.org/10.1186/s12917-020-02508-y
3. Dong WL, Kong LC, Wang Y, Gou CL, Xu B, Ma HX, Gao YH. 2017. Aminoglycoside resistance of *Trueperella pyogenes* isolated from pigs in China. J Vet Med Sci 79:1836–1839. https://doi.org/10.1292/jvms.16-0597
4. Rzewuska M, Czopowicz M, Gawryś M, Markowska-Daniel I, Bielecki W. 2016. Relationships between antimicrobial resistance, distribution of virulence factor genes and the origin of *Trueperella pyogenes* isolated from domestic animals and European bison (*Bison bonasus*). Microb Pathog 96:35–41. https://doi.org/10.1016/j.micpath.2016.05.001
5. Jarosz ŁS, Gradzki Z, Kalinowski M. 2014. *Trueperella pyogenes* infections in swine: clinical course and pathology. Pol J Vet Sci 17:395–404. https://doi.org/10.2478/pjvs-2014-0055
6. Ribeiro MG, Risseti RM, Bolaños CAD, Caffaro KA, de Morais ACB, Lara GHB, Zamprogna TO, Paes AC, Listoni FJP, Franco MMJ. 2015. *Trueperella pyogenes* multispecies infections in domestic animals: a retrospective study of 144 cases (2002 to 2012). Vet Q 35:82–87. https://doi.org/10.1080/01652176.2015.1022667
7. Ganesan S, Comstock AT, Sajjan US. 2013. Barrier function of airway tract epithelium. Tissue Barriers 1:e24997. https://doi.org/10.4161/tisb.24997
8. Lam E, Ramke M, Groos S, Warnecke G, Heim A. 2011. A differentiated porcine bronchial epithelial cell culture model for studying human adenovirus tropism and virulence. J Virol Methods 178:117–123. https://doi.org/10.1016/j.jviromet.2011.08.025
9. Wu N-H, Yang W, Beineke A, Dijkman R, Matrosovich M, Baumgärtner W, Thiel V, Valentin-Weigand P, Meng F, Herrler G. 2016. The differentiated airway epithelium infected by influenza viruses maintains the barrier function despite a dramatic loss of ciliated cells. Sci Rep 6:39668. https://doi.org/10.1038/srep39668
10. Meng F, Wu N-H, Seitz M, Herrler G, Valentin-Weigand P. 2016. Efficient suilysin-mediated invasion and apoptosis in porcine respiratory epithelial cells after streptococcal infection under air-liquid interface conditions. Sci Rep 6:26748. https://doi.org/10.1038/srep26748
11. Meng F, Tong J, Vötsch D, Peng J-Y, Cai X, Willenborg M, Herrler G, Wu N-H, Valentin-Weigand P, Palmer GH. 2019. Viral coinfection replaces effects of suilysin on *Streptococcus suis* adherence to and invasion of respiratory epithelial cells grown under air-liquid interface conditions. Infect Immun 87:e00350-19. https://doi.org/10.1128/IAI.00350-19
12. Meng F, Punyadarsaniya D, Uhlenbruck S, Hennig-Pauka I, Schwegmann-Wessels C, Ren X, Dürrwald R, Herrler G. 2013. Replication characteristics of swine influenza viruses in precision-cut lung slices reflect the virulence properties of the viruses. Vet Res 44:110. https://doi.org/10.1186/1297-9716-44-110
13. Fiole D, Deman P, Trescos Y, Mayol JF, Mathieu J, Vial JC, Douady J, Tournier JN. 2014. Two-photon Intravital imaging of lungs during anthrax infection reveals long-lasting macrophage-dendritic cell contacts. Infect Immun 82:864–872. https://doi.org/10.1128/IAI.01184-13
14. Ågren L, Elfsmark L, Akfur C, Jonasson S. 2021. High concentrations of ammonia induced cytotoxicity and bronchoconstriction in a precision-cut lung slices rat model. Toxicol Lett 349:51–60. https://doi.org/10.1016/j.toxlet.2021.06.001
15. Delgado-Ortega M, Melo S, Punyadarsaniya D, Ramé C, Olivier M, Soubieux D, Marc D, Simon G, Herrler G, Berri M, Dupont J, Meurens F. 2014. Innate immune response to a H3N2 subtype swine influenza virus in newborn porcine trachea cells, alveolar macrophages, and precision-cut lung slices. Vet Res 45:42. https://doi.org/10.1186/1297-9716-45-42
16. Wu W, Zhang W, Booth JL, Metcalf JP, Chan MCW. 2012. Influenza A(H1N1)pdm09 virus suppresses RIG-I initiated innate antiviral responses in the human lung. PLoS ONE 7:e49856. https://doi.org/10.1371/journal.pone.0049856
17. Qin L, Meng F, He H, Yang Y-B, Wang G, Tang Y-D, Sun M, Zhang W, Cai X, Wang S. 2021. A virulent *Trueperella pyogenes* isolate, which causes severe bronchoconstriction in porcine precision-cut lung slices. Front Vet Sci 8:824349. https://doi.org/10.3389/fvets.2021.824349
18. Farsani SMJ, Deijs M, Dijkman R, Molenkamp R, Jeeninga RE, Ieven M, Goossens H, van der Hoek L. 2015. Culturing of respiratory viruses in well-differentiated pseudostratified human airway epithelium as a tool to detect unknown viruses. Influenza Other Respir Viruses 9:51–57. https://doi.org/10.1111/irv.12297
19. Meng F, Wu NH, Nerlich A, Herrler G, Valentin-Weigand P, Seitz M. 2015. Dynamic virus-bacterium interactions in a porcine precision-cut lung slice coinfection model: swine influenza virus paves the way for *Streptococcus suis* infection in a two-step process. Infect Immun 83:2806–2815. https://doi.org/10.1128/IAI.00171-15
20. Su A, Tong J, Fu Y, Müller S, Weldearegay YB, Becher P, Valentin-Weigand P, Meens J, Herrler G. 2020. Infection of bovine well-differentiated airway epithelial cells by *Pasteurella multocida*: actions and counteractions in the bacteria-host interactions. Vet Res 51:140. https://doi.org/10.1186/s13567-020-00861-2
21. Jost BH, Trinh HT, Songer JG, Billington SJ. 2003. Immunization with genetic toxoids of the *Arcanobacterium pyogenes* cholesterol-dependent cytolysin, pyolysin, protects mice against infection. Infect Immun 71:2966–2969. https://doi.org/10.1128/IAI.71.5.2966-2969.2003
22. Remot A, Descamps D, Noordine ML, Boukadiri A, Mathieu E, Robert V, Riffault S, Lambrecht B, Langella P, Hammad H, Thomas M. 2017. Bacteria isolated from lung modulate asthma susceptibility in mice. ISME J 11:1061–1074. https://doi.org/10.1038/ismej.2016.181
23. Bryson KJ, Garrido D, Esposito M, McLachlan G, Digard P, Schouler C, Guabiraba R, Trapp S, Vervelde L. 2020. Precision cut lung slices: a novel versatile tool to examine host-pathogen interaction in the chicken lung. Vet Res 51:2. https://doi.org/10.1186/s13567-019-0733-0
24. Oh CK, Geba GP, Molfino N. 2010. Investigational therapeutics targeting the IL-4/IL-13/STAT-6 pathway for the treatment of asthma. Eur Respir Rev 19:46–54. https://doi.org/10.1183/09059180.00007609
25. Huffnagle GB, Dickson RP. 2015. The bacterial microbiota in inflammatory lung diseases. Clin Immunol 159:177–182. https://doi.org/10.1016/j.clim.2015.05.022
26. Dai J, Shen J, Chai Y, Chen H. 2021. IL-1β impaired diabetic wound healing by regulating MMP-2 and MMP-9 through the p38 pathway. Mediators Inflamm 2021:6645766. https://doi.org/10.1155/2021/6645766
27. Harris J, VanPatten S, Deen NS, Al-Abed Y, Morand EF. 2019. Rediscovering MIF: new tricks for an old cytokine. Trends Immunol 40:447–462. https://doi.org/10.1016/j.it.2019.03.002